

Application of a Perturbation Recycling Method in the Large-Eddy Simulation of a Mesoscale Convective Internal Boundary Layer

SHANE D. MAYOR*

Department of Atmospheric and Oceanic Sciences, University of Wisconsin—Madison, Madison, Wisconsin

PHILIPPE R. SPALART

Boeing Commercial Airplanes, Seattle, Washington

GREGORY J. TRIPOLI

Department of Atmospheric and Oceanic Sciences, University of Wisconsin—Madison, Madison, Wisconsin

(Manuscript received 26 June 2001, in final form 7 January 2002)

ABSTRACT

An arrangement of boundary conditions is described and demonstrated that facilitates the large-eddy simulation (LES) of inhomogeneous boundary layers such as internal boundary layers. In addition to the domain where the internal boundary layer develops, the method requires a section of domain over the upwind surface that is of the order of 10 boundary layer thicknesses and thus similar in size to that needed for the LES of the upwind boundary layer. In addition to periodic lateral, closed upstream, and open downstream boundary conditions, a simple and efficient perturbation recycling technique, which follows from one of Lund, Wu, and Squires, is used to generate a steady supply of fully developed turbulence from the inflow boundary. The arrangement is used to simulate a convective internal boundary layer during a cold-air outbreak over water. Results show the method consistently produces a solution that is homogeneous over the upwind surface and inhomogeneous over the downwind surface, and that the statistics are stationary after spinup. The sensitivity to the placement of the outflow boundary is tested, and examples of instantaneous and mean fields generated by the simulations are shown.

1. Introduction

Internal boundary layers (IBLs) are associated with abrupt spatial changes in one or more surface properties such as temperature or roughness (Mahrt 2000). A classic example is cold offshore flow over a relatively warm and vast body of water. The internal boundary layer begins at the shore and eventually engulfs the entire preexisting boundary layer at some offshore distance, typically a few kilometers. Garrett (1990) calls this a *mesoscale* internal boundary layer in contrast to a *local* internal boundary layer that does not engulf the preexisting boundary layer. Our goal is a realistic large-eddy simulation (LES) of a mesoscale internal boundary layer at a manageable computational cost. The method

we describe could easily be used to simulate a local internal boundary layer also.

One approach used previously (for an example, see Lin et al. 1997) is to simulate a horizontally homogeneous boundary layer in which the entire surface boundary condition is altered at some point in time. This Lagrangian approach assumes that the temporal evolution of turbulence is equivalent to the spatial evolution given an assumed advection velocity. This approach allows the use of spectral solutions in the horizontal directions (Moeng 1984). It is a convenient and numerically accurate method, but it lacks the physical realism of a spatially evolving boundary layer. Fourier spectral methods require periodic (cyclic) lateral boundary conditions.

It is possible to generate horizontally inhomogeneous turbulence using horizontally periodic domains, but it introduces limitations. Glendening (1995), for example, presents an LES of a plume emanating from a narrow Arctic lead (a crack in the sea ice). In his case, the atmosphere upwind of the lead is assumed to be very stable. The flow is from the left. The left 200 m of the domain lies over a water surface and the right 300 m

* Current affiliation: National Center for Atmospheric Research, Advanced Studies Program, Boulder, Colorado.

Corresponding author address: Dr. Shane D. Mayor, Advanced Studies Program, National Center for Atmospheric Research, P.O. Box 3000, Boulder, CO 80307-3000.
E-mail: shane@ucar.edu

over ice. The lead creates a buoyant plume above and downstream of itself. This modeling approach works if the atmosphere upwind of the lead is not turbulent and the LES handles the transition from nonturbulent to turbulent flow correctly. Furthermore, because of the periodic domain, only model results from a period prior to the time when the plume re-enters the domain over the lead can be used. We prefer to have an unlimited time sample.

In a more recent paper, Glendening and Lin (2002) use a periodic domain divided into two equal areas each of different surface roughnesses. They allow the simulation to run long beyond the time it takes for a parcel of air to advect across the entire domain. This style of simulation is analogous to simulating over an infinite plane with a patchwork of two surface roughnesses—each patch contributing a local internal boundary layer. It is a good example of what might happen over a large agricultural region with two types of crops.

The *spatial* simulation of mesoscale internal boundary layers requires a different approach. A domain that is periodic in the direction perpendicular to the shore can only be used if the flow crossing the outflow boundary is restored to the mean properties of the boundary layer over the upwind surface. Although this can be done both if the turbulence is preserved or suppressed [see Spalart and Watmuff (1993) for examples of the *fringe method* in engineering applications], the method failed to spread widely. Drawbacks include the need to finely adjust a number of parameters for each new case, and limitations in how much the freestream conditions can differ between the inflow and outflow boundaries. Therefore, a simpler and more general method to generate a homogeneous fully developed turbulent boundary layer before the flow reaches the change in surface conditions is desired.

An alternative to a periodic boundary is an *open boundary*. Several methods for open boundary conditions have been proposed and are used routinely in mesoscale models. They are based on the philosophy of the Sommerfeld radiation condition whereby both waves and other perturbations are allowed to pass out of the domain while no waves or other perturbations can be advected in. It is set up by having one variable, usually the normal component of velocity, specified by a radiative wave tendency equation given by Orlanski (1976) on the boundary while all other variables except one (usually pressure) are specified by the assumption of zero normal gradient. This condition allows for some, often unchecked, evolution of structure in the tangential direction to the boundary, and for (sometimes destructive) trends in net mass inflow or outflow.

To maintain the mean thermodynamic and wind profile upstream of the IBL, it is necessary to impose a *closed* (or hard) condition on the inflow, where the flow is held constant in the mean according to prescribed boundary conditions. Although the inflow conditions remain constant, they will reflect upstream propagating waves and any outflowing advecting perturbations. In

addition, the inflowing air will forever remain unperturbed resulting in the need for a large spinup¹ region downwind of the boundary before the modeled turbulence reaches maturity.

The use of combined *open downstream* and *closed upstream* boundary conditions (ODCU) is often employed in the field of wind engineering such as Fedorovich et al. (2001). They employed an LES to duplicate wind tunnel experiments of a spatially evolving convective boundary layer. They added uncorrelated random values to the inflow condition to simulate the effect of perturbations in the experimental flow. This cannot generate very realistic turbulence even if separate random sequences are used to obtain the off-diagonal Reynolds stresses because the phase relationships between components (roughly put, the shape of the eddies) are incorrect. As a result, the flow needs to complete a relatively irrelevant transition process, whether from small or finite perturbations, within the simulated domain. However, their use of an upstream inflow boundary is justified because that is effectively what a wind tunnel provides. The atmosphere, on the other hand, has no lateral boundaries and features upstream propagating waves such as gravity waves, acoustic waves, and sheared wind profiles, which lessen the chances of success of having a pure inflow boundary. For the real atmosphere, a hard upstream boundary is typically not appropriate. For an overview of boundary conditions used in atmospheric models we refer the reader to Duran (1999) and Pielke (2001).

There are certain atmospheric flow problems, however, where ODCU conditions could be effectively employed. These situations involve a convective or neutral boundary layer with almost unidirectional flow where waves in the stable air above the boundary layer are ignored. Even for this application, the ODCU condition as proposed by Fedorovich et al. (2001) will require a large region for turbulence maturation that limits its usefulness compared to alternatives. In this study, we employ a technique to economically solve the turbulence maturation limitation of the ODCU condition using a perturbation recycling technique designed to allow turbulence to mature in a short simulation region.

2. Description of domain and boundary conditions

The total size of the domain and gridpoint spacing required for an LES depend on the depth of the boundary layer to be simulated. For the case we present here, the boundary layer is 400 m deep. The flow is from the west-northwest and the shoreline oriented north-south. Therefore, we chose 15-m gridpoint spacing and a domain that is 1.8 km in the north-south direction by 11.685 km in the east-west direction. The depth of the domain is 1 km. The total number of grid points is 6.45

¹ The word *spinup* in large-eddy simulation research refers to the time or space necessary to generate mature turbulence from a nonturbulent initial condition.

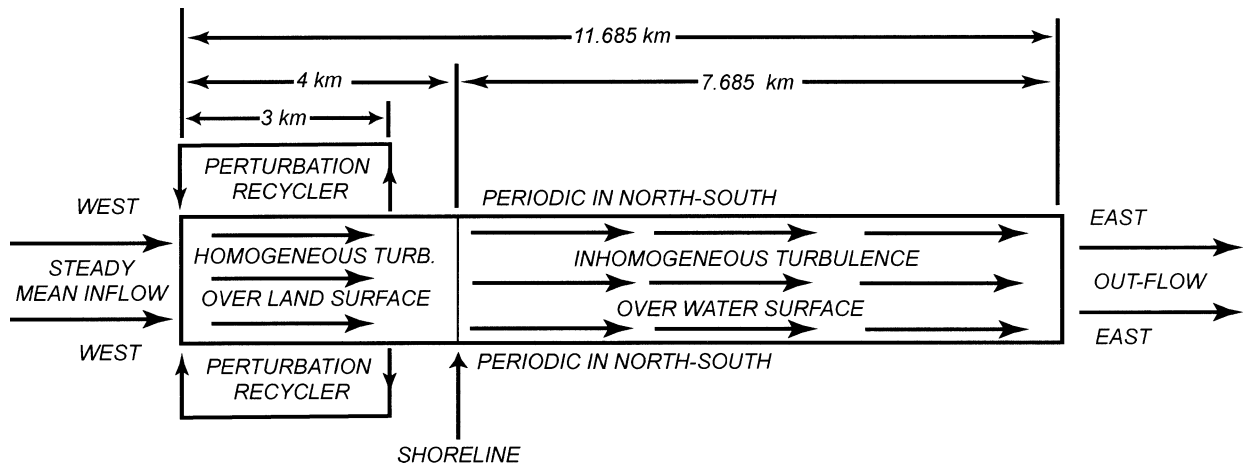


FIG. 1. Plan view of the IBL domain with *perturbation recycler*. The boundary layer over land (left 4 km) is homogeneous while the boundary layer over water (right 8 km) is inhomogeneous.

million. The western 4 km of the domain employs a land surface parameterization designed to model the surface fluxes upwind of the internal boundary layer. The remaining 7.685 km of domain uses a water surface parameterization that is set to model the surface fluxes that drive the internal boundary layer. Figure 1 shows a plan view of the IBL domain. The domain is periodic only in the shore-parallel (north-south) direction.

The turbulent inflow method we use is modified from one described by Lund et al. (1998) and originally inspired by that of Spalart (1988). The objective of their simulations is to model the spatial development of shear-generated (mechanical) boundary layers for applications in engineering. Their motivation for insisting on spatial direct numerical simulation (DNS) and LES is their interest in strong pressure gradients, bumps, corners, and eventually separation. These are not accommodated by temporal techniques, nor by Spalart's (1988) method for that matter.

The inflow boundary condition for each predicted variable on the western side is composed of a mean and a perturbation. The mean at each altitude on the inflow wall is obtained from the solution of a precursor run (discussed at end of this section). The mean is held constant during the entire IBL simulation. Perturbations on the inflow wall are obtained from a single vertical plane of grid points several kilometers downstream of the inflow wall. The vertical plane of grid points, which we call the *magic slice*, is oriented parallel to, and upstream of, the shoreline. In the form of an equation, the upwind boundary condition can be written as

$$A_{\text{inflow}} = \overline{A_{\text{precursor}}} + A'_{\text{downstream}}, \quad (1)$$

where A is any predicted variable, the overbar represents the mean, and the prime a perturbation.

At each time step during the simulation, turbulent perturbations of all variables are copied from the magic slice to the inflow wall. The perturbations are deviations from the mean at each altitude on the magic slice. The

perturbations are added to the corresponding grid point on the inflow wall. This is the key idea due to Lund et al. (1998) and it produces realistic fluctuations on the inflow boundary that do not need a long relaxation at all before becoming quality turbulence. Engineering boundary layers grow in thickness, so the vertical plane of perturbations must be compressed in the direction normal to the surface before being added to the mean inflow at the upstream boundary in those applications. For atmospheric applications, a temperature inversion keeps the boundary layer height approximately constant upwind of the discontinuity, making the compression unnecessary. The result is a homogeneous boundary layer over the upwind section of the domain that advects over the downwind section where it undergoes evolution. The position of the magic slice appears to be arbitrary as long as it is far enough from the inflow boundary to allow decorrelation of the perturbations before they are recycled. For the results presented here, the position of the magic slice was 3 km east of the inflow boundary, or about eight boundary layer thicknesses. This was so that the turbulence characteristics in that section would remain approximately the same as those in the precursor simulation that was also 3 km long in the east-west direction. Figure 2 shows the temporal autocorrelation function for vertical velocity at 200 m. It shows that the turbulence structures are completely decorrelated within about 2 min. The mean wind speed at 200 m was about 7 m s^{-1} and, therefore, it would take a parcel more than 7 min to advect 3 km.

In order to allow the free passage of all flow perturbations out of the boundaries, we must use an open boundary condition. In classical engineering problems, where incompressible formulations are often used and static stability is not considered, the problem is simpler. Physical waves can propagate upstream only very weakly so that the flow can be fixed at the upstream boundary and some kind of upstream differencing can be used on

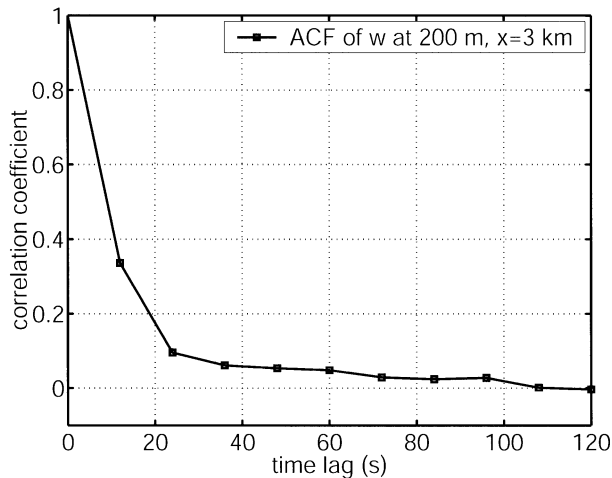


FIG. 2. Average temporal autocorrelation function (ACF) of vertical velocity at 200-m altitude and 3 km west of the inflow wall. Sixty time series, each containing 233 values, at 12-s intervals were used to compute this function.

the downstream boundary. Atmospheric flow problems, however, contain the added complication of static stability that allows for both upstream and downstream propagating gravity waves. Compressible models have the added factor of upstream and downstream acoustic waves. Tripoli and Cotton (1982) discussed the problem of radiating acoustic waves in some depth. Typically one makes no attempt to allow acoustic waves to move out laterally, and we have not here. Rossby or vorticity waves are also present when Coriolis is added but they are negligible on the small LES domain of this study.

Gravity waves, however, must be allowed to escape and can move out of the domain upstream or downstream. The simulation discussed here was designed with a strong vertical damping above the boundary layer designed to remove most gravity waves and prevent deep fast moving waves. As a result, no vertical gravity wave modes exist that can support a gravity wave phase speed that exceeds the westerly flow speed of this problem. If important, and if westward-propagating gravity waves did exist, the perturbation recycler would not be able to properly represent their movement.

In this study, eastward-propagating gravity waves and flow perturbations are allowed to escape through the eastern boundary using a gravity wave radiation condition discussed by Durran (1981). This gravity wave radiation condition is a member of a class of gravity wave radiation boundary conditions of varying complexities developed by Orlanski (1976), Klemp and Wilhelmson (1978), Durran (1981), and Hack and Schubert (1981). The general form of the boundary condition is to replace the normal velocity tendency at the boundary with

$$\frac{\partial u}{\partial t} = -(c_g + u) \frac{\partial u}{\partial x} = -u^* \frac{\partial u}{\partial x}. \quad (2)$$

Here, c_g is the gravity wave phase speed, *always directed out of the boundary*, and $u^* = c_g + u$ is the Doppler-shifted phase speed. In the case of the original Orlanski method, the radiation condition is applied to all predicted variables. However, it was later shown by Klemp and Wilhelmson (1978) that this method is an over specification that can be avoided by applying this condition only to the normal velocity. All other variables, except one (normally the pressure variable) are predicted with forward upstream differencing for outflow and held constant for inflow, determined by the sign of u . For pressure, the governing equations do not require the specification of a pressure boundary condition. We also apply the radiation condition in this way.

For the application of the radiation condition to the u equation, forward upstream differencing is used for outflow while u is held constant for inflow and where inflow or outflow is determined by the sign of u^* . The problem remaining is determining c_g , where many vertical modes of internal gravity waves exist all with different phase speeds. Orlanski suggested a method by which the radiation condition equation is applied one grid point in from the boundary, at a past time level where one can diagnose c_g by knowing the time tendency of u . The diagnostic equation for c_g is formulated as

$$u_o^* = \frac{\Delta x u'_{b-1} - u_{b-1}^{t-1}}{\Delta t u_{b-1}^{t-1} - u_{b-2}^{t-1}}, \quad (3)$$

where u_o^* is the ‘‘Orlanski’’ Doppler-shifted phase speed, b represents the boundary grid index, t represents the current time level, Δx is the grid spacing, and Δt is the time step.

This method tends to suffer, however, from a tendency toward the formation of an unchecked bias to outflow or inflow that then leads to domain mass trend over time. For instance, in regions of outflow, the gravity wave propagation speed and the advection velocity are both directed outward while in regions of inflow they oppose each other. Therefore, the outflow boundary condition will be biased toward flow perturbations within the outflow stream. Hence, one can develop a bias toward inflow or outflow that raises the domain integral mass with no compensating forces to reverse the trend.

This problem is more amplified the smaller the domain, making it most problematic to LES applications. Successful applications of the Orlanski method have, historically, been limited mostly to incompressible or anelastic models (see Clark 1977) where systematic domain-scale momentum convergence is forbidden. Historically, most LES models have also been incompressible or anelastic. In elastic models, such as the one used in this study, these biases lead to systematic domain-scale pressure rises or falls. Klemp and Wilhelmson (1978) suggested that c_g could be adequately set to a single (dominant) gravity phase speed. This reduces the problem of domain-scale mass trending considerably by limiting the variability of c_g^* , but does not eliminate it.

Unfortunately, mass trending is quite noticeable with the Klemp and Wilhelmson (1978) condition when applied to LES.

The Hack and Schubert (1981) technique for this boundary condition involves the use of normal modes, effectively applying the boundary condition to each vertical gravity wave mode using its own unique phase speed. Unfortunately, this condition too does not solve the mass trending problem. Boersma (1998) discusses an alternative approach to determine u^* by enforcing global mass conservation.

The Durran (1981) method, used here, is derived from a method reported by Klemp and Lilly (1978) and is a reasonable compromise that helps minimize the mass trending problem, but is also less effective in allowing outward radiation of gravity waves. The idea is to use the Orlanski method to diagnose an effective u^* at all heights in the vertical column and then use a constant value of u^* based on the u^* -weighted vertical average of u^* . This averaging procedure can be written as

$$u_D^* = \frac{\Delta x \sum_{k=1}^{n_z} (u_{b-1}^{t-1} - u_{b-1}^{t-2}) \text{sign}(u_{b-1}^{t-1} - u_{b-2}^{t-1})}{\Delta t \sum_{k=1}^{n_z} |u_{b-1}^{t-1} - u_{b-2}^{t-1}|}, \quad (4)$$

where u_D^* is the Durran Doppler-shifted phase speed that is constant with height, and n_z is the number of vertical levels. This method does not have optimal wave radiation characteristics, but it nevertheless produces acceptable gravity wave transmission. The predicted flow in the vertical grid column normal to the boundary becomes a linear combination of the predicted normal flow at one column inward and the normal flow predicted at the boundary grid column. This effectively preserves the inflow–outflow relationship of the interior column at the boundary column. It was found that applying this condition reduces domain-scale mass trending to acceptable levels, even in the LES applications.

A numerical technique is applied to the top eight grid points across the entire domain to damp the reflection of gravity waves and prevent the formation of deep fast-moving vertical gravity wave modes. We do this to isolate the turbulence processes in the boundary layer, realizing that the observed structures are possibly tied to the gravity waves we eliminate. The damping is prescribed as a term added to each predicted equation in the form

$$\text{DAMPING}_A = -\frac{A - A_0}{\tau(z)}, \quad (5)$$

where A is the predictive variable, A_0 is the reference (undisturbed) state of that variable, and $\tau(z)$ is the relaxation timescale defined to linearly increase from some height z_D to the model-top height z_H using the relationship

$$\tau(z) = \tau_0 \frac{z - z_D}{z_H - z_D}. \quad (6)$$

We set $\tau_0 = 10$ s.

Prior to running the IBL domain, we spin up turbulence in a smaller, doubly periodic, domain that is only 1.8 by 3 km wide and 1 km tall. The surface parameterization of this *precursor* simulation is set to model the surface fluxes over the land. The precursor simulation is initialized horizontally homogeneous according to a vertical profile representative of the observed mean conditions there. Finite random perturbations are added to the initial velocity field to seed instabilities and help speed the development of turbulence. When the total domain turbulent kinetic energy becomes quasi-stationary, the precursor simulation is stopped and its final three-dimensional flow field is replicated over the longer dimension of the IBL domain. The one-dimensional mean profile of the precursor run's 30-min solution is also used as the mean inflow profile, as discussed above.

3. Demonstration of method

As a demonstration of the technique, we use the University of Wisconsin's Nonhydrostatic Modeling System as the LES code (Tripoli 1992). We have run the code with parameters to simulate a purely convective boundary layer and an Ekman boundary layer and get results very comparable to those found in Nieuwstadt et al. (1993) and Andren et al. (1994; see also Coleman et al. 1990). Here, we present our first results of a convective internal boundary layer for a cold air outbreak case observed on 13 January 1998 on the western shore of Lake Michigan. On this day air temperatures near the surface were approximately -20°C and the mean boundary layer flow was from the west-northwest at $5\text{--}10$ m s^{-1} . Skies were clear over the land and for the first few kilometers offshore.

The horizontally homogeneous initial conditions of the precursor simulation are based on observations collected by a National Center for Atmospheric Research (NCAR) Integrated Sounding System (ISS) that was located 10 km upstream of the shore. Temperature and dewpoint data obtained from a radiosonde launched at 1630 UTC (right panel in Fig. 3) indicate a well-mixed boundary layer up to about 365 m. A strong capping inversion existed above 400 m. The increase of potential temperature in this capping inversion layer is $2.6^\circ (100 \text{ m})^{-1}$. Range–height indicator (RHI) scans from the University of Wisconsin's volume imaging lidar confirm the presence of a mixed layer at the coast with an entrainment zone between approximately 300 and 500 m above the surface. The diamonds in the left and center panels of Fig. 3, at altitudes between 207 and 543 m AGL, represent wind measurements from a 915-MHz boundary layer profiler. These winds, with 60-m vertical resolution, are a consensus of data collected between 1635 and 1651 UTC. In addition to the radiosonde and

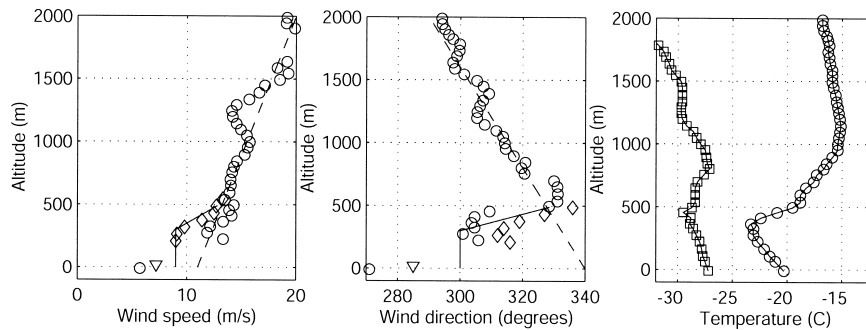


FIG. 3. Vertical profiles of wind speed (left), wind direction (center), and temperature and dewpoint (right) from observations. In the left and center panels, circles are for radiosonde data, diamonds are for radar wind profiler data, and the upside down triangle is for surface observations, the solid line represents the initial condition to the precursor simulation and the dashed line represents the geostrophic wind profile. The circle at zero height in the left and center panels is an observation from the NCAR ISS tower. In the right panel, circles are for temperature and squares are for dewpoint.

profiler data, two observations of wind speed and direction are included near the surface on Fig. 3. The first is from the NCAR ISS tower and is plotted as circle. The second is from the National Oceanic and Atmospheric Administration (NOAA) weather station SGNW3 that was located at the shore and is plotted as an upside-down triangle. The SGNW3 temperature and dewpoint observations at 1630 UTC match those from the ISS to within 1° . Because of the sampling errors in radiosonde and radar profiler wind measurements, the wind speed and direction profile used to initialize the model was obtained from a subjective (piecewise) linear fit among these data as described next.

The mean wind profile for initialization is constructed in three parts. Above 500 m, we assume that the observed wind profile is geostrophic. We fit a straight line to the wind data above 500 m and extrapolate the geostrophic values in the mixed layer. This geostrophic reference state specifies the large-scale pressure gradient as described by Tripoli and Cotton (1989). Below 300 m, where the boundary layer is well mixed, we set the speed and direction constant. Between 300 and 500 m, where the sounding is weakly stable, we interpolate between the constant value below and the geostrophic value at 500 m. The exact initial wind profile for the horizontally homogeneous initial condition ceases to be important because the model will adjust to a quasi-equilibrium with unique mean properties after large eddies are formed. Random perturbations of $\pm 0.5 \text{ m s}^{-1}$ were added to all three velocity components at all grid points below 450 m to speed the development of eddies in the precursor simulation.

The land surface parameterization scheme used an albedo of 0.66 to represent partially snow-covered land and cause the temporal warming rate at the bottom of the model over land to match those observed at the upwind observation site. Therefore, the upwind boundary layer was weakly convective. The precursor simulation was stopped 30 min after initialization. Figure 4

shows the vertical velocity on horizontal and vertical planes in the precursor boundary layer 30 min after initialization. The 30-min solution of the precursor simulation was replicated four times in the IBL domain as the initial condition. This minimizes the time required to spin up the IBL domain. The IBL domain was run for 1 h, so that a particle outside the boundary layer traveled over twice the length of the domain during the simulation. The temperature of the water surface parameterization was held at 6°C .

4. Discussion of results

Figure 5 shows the vertical velocity on vertical and horizontal planes in the IBL domain after 30 min of simulation. The horizontal plane in Fig. 5 is at 200 m above the surface and it shows lineal structures that are aligned parallel to the mean wind at that level. The lineal features are most organized over the land and become less well organized over the lake with the intensification of convection. The horizontal spacing of these lineal structures is between 600 m and 1 km. Figure 6 shows the relative humidity on vertical and horizontal planes in the IBL domain. The horizontal plane in Fig. 6 is at 7.5 m above the surface (the lowest atmospheric grid point in the model) and it shows more closely lineal structures over the land and cellular structures over the water. Cellular structures have been also observed in the aerosol backscatter field obtained by horizontal lidar scans on this date and location (see Mayor and Eloranta 2001). The contour lines in the top panel of Figs. 5 and 6 are of potential temperature at 1.5-K intervals. The potential temperature contours are provided to indicate the location of the capping inversion.

To determine the stationarity of the turbulence statistics in the IBL domain, we computed and averaged the turbulent kinetic energy (TKE) over two 3-km-long sections of the domain as a function of time. The first section included the grid points from the inflow bound-

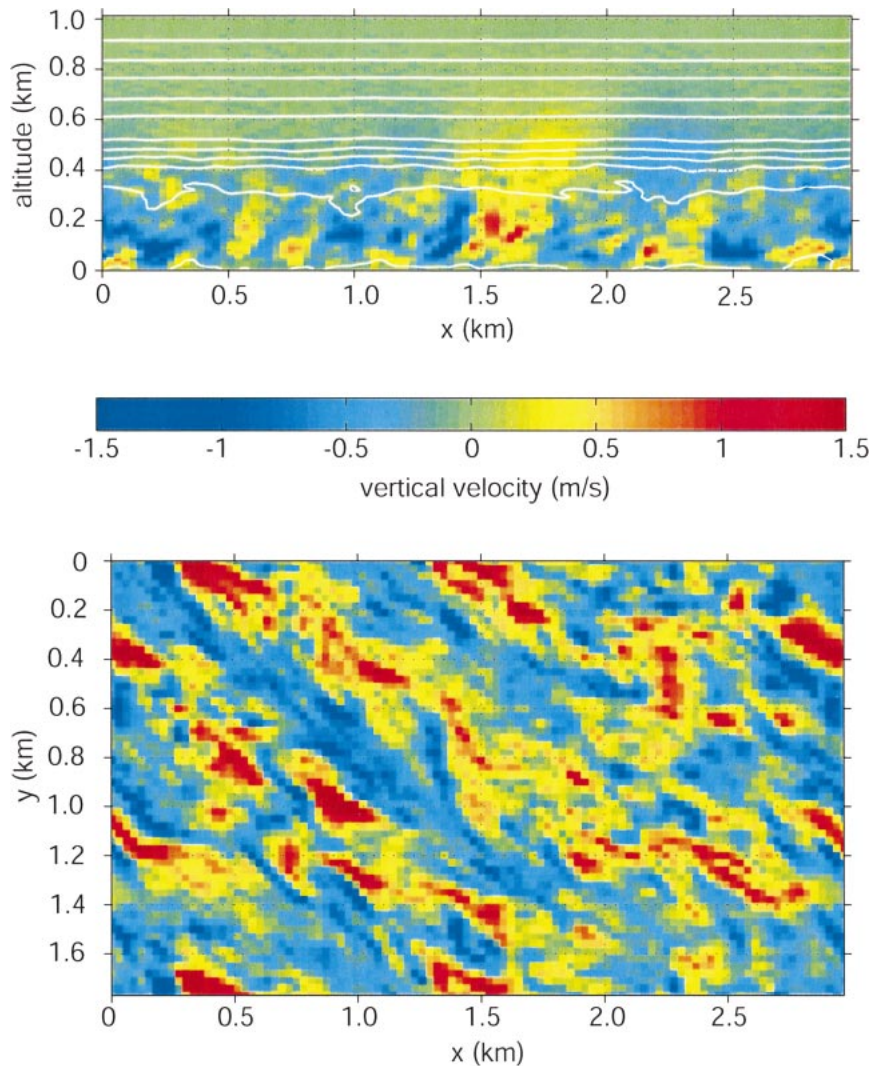


FIG. 4. Vertical velocity on (top) vertical and (bottom) horizontal slices through the precursor domain 30 min after initialization. In the top panel the z axis has been expanded and the contours are of potential temperature at 1.5-K intervals. The horizontal slice in the bottom panel is located at 200 m AGL.

ary to 3 km downstream of the inflow boundary and is plotted as the dash-dot line in Fig. 7. The turbulence in this section, which is entirely over land, and 1 km upstream of the lake, remains stationary (as expected) during the full 60-min IBL simulation. The second section includes the grid points from 4 to 7 km offshore and is indicated by a solid line in Fig. 7. At the beginning of the simulation its value is the same as that over the land, but it quickly triples and levels off within 10 min. Therefore, the turbulence structure over the water exhibits stationarity during the simulation starting at about 10 min after initialization. For comparison, the dashed line in Fig. 7 is the TKE averaged over the entire precursor domain as a function of time. It shows an exponential-like increase until 20 min after initialization, when it levels off.

We present Fig. 8 to show the homogeneity of turbulence over the land and the inhomogeneity of turbulence over the water. The solid line in Fig. 8 was constructed by averaging the TKE on shore-parallel vertical slices as a function of distance from the shore during the period between 10 and 50 min after initialization. It shows us that the turbulence is very homogeneous over the land and triples within about 3 km of the shore over the water. For comparison, the dashed line in Fig. 8 is the average TKE from an LES with doubly periodic lateral boundary conditions that was started with the 30-min solution of the precursor run and continued with the water surface parameterization. The offshore distance was estimated by multiplying the time of each frame by 7 m s^{-1} , which is an estimate of the mean wind speed in the middle of the boundary

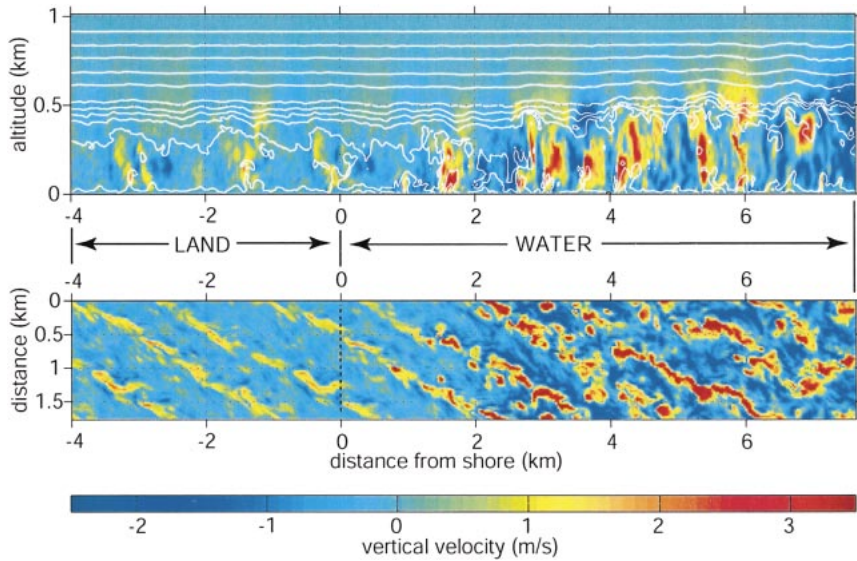


FIG. 5. Vertical velocity on (top) vertical and (bottom) horizontal planes in the IBL domain 30 min after initialization. In the top panel the vertical axis has been expanded and the contours are of potential temperature at 1.5-K intervals. The horizontal slice in the bottom panel is located at 200 m above the surface.

layer. The dashed curve shows a similar increase in TKE over the first 3 km offshore, but it does peak with a larger value and appears to remain less steady for equivalent distances greater than 4 km offshore.

To test the sensitivity of the TKE to the position of the open outflow boundary condition, we ran another simulation with the outflow wall moved in to 5.685 km offshore. We call this the *shifted IBL domain* and have

plotted the mean TKE as a function of offshore distance for it as the dotted curve in Fig. 8. The curve is extremely similar to the one from the IBL domain that extends out to 7.685 km offshore, lending credibility to the robustness of the technique. However, both curves show a slight (<10%) downward pointing tail within 150 m of the outflow boundary. Although seeing this common trait in only two simulations is not sufficient

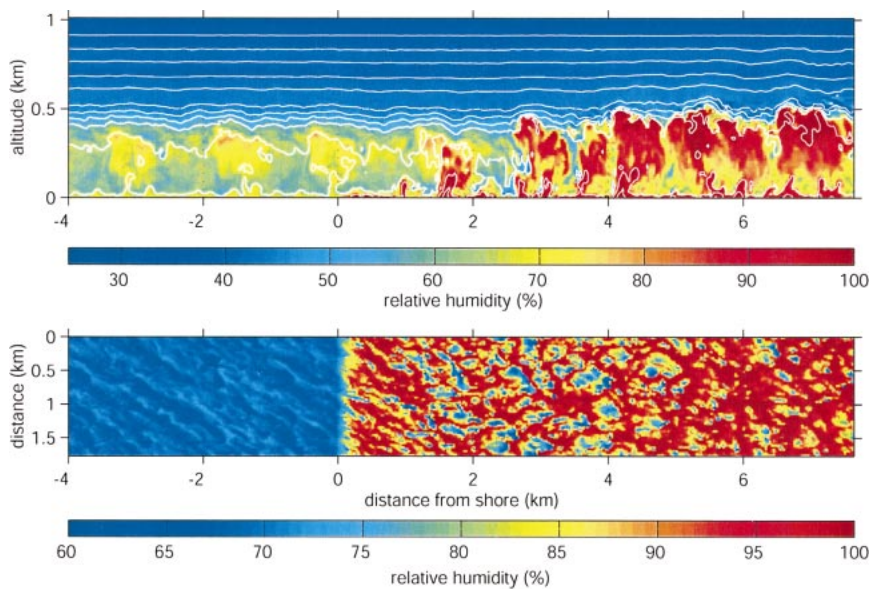


FIG. 6. Relative humidity on (top) vertical and (bottom) horizontal planes in the IBL domain 30 min after initialization. In the top panel, the vertical axis has been expanded and the contours are of potential temperature at 1.5-K intervals. The horizontal plane in the bottom panel is located 7.5 m above the surface.

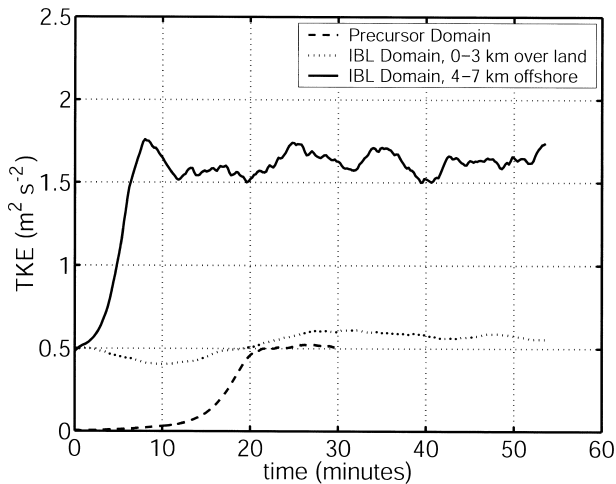


FIG. 7. Mean turbulent kinetic energy as a function of time for the precursor domain (dashed line), and upwind (dotted line) and downwind (solid line) portions of the IBL domain.

to call it a systematic bias, it is entirely conceivable that it is the result of the outflow boundary condition. Fortunately, it affects only a very small part of the domain and can easily be excluded, as we did, when computing turbulence statistics over the downwind region.

The simulation output can also be used to investigate the mean properties of the boundary layer transition. Figure 9 shows contours of mean wind direction, speed, potential temperature and relative humidity on shore-perpendicular vertical cross sections. Perhaps the most pronounced feature in these plots is the slight dip in the height of the inversion within the first 4 km offshore presumably caused by divergent flow associated with acceleration in the mixed layer. Similarly, in engineering boundary layers, at laminar/turbulent transitions, the momentum thickness is unchanged and the displacement thickness decreases. The acceleration in our case is caused by a redistribution of momentum by convection and a reduction of surface roughness over the water. Within the mixed layer, gradual increases in potential temperature and relative humidity occur at constant altitudes in the mixed layer as one moves offshore. The simulation indicates that the surface momentum flux for this particular case decreased from $0.44 \text{ kg m}^{-1} \text{ s}^{-2}$ to $0.25 \text{ kg m}^{-1} \text{ s}^{-2}$ over the water. The surface sensible heat flux increased from 40 to over 800 W m^{-2} and the latent heat flux increased from 30 to 400 W m^{-2} . Therefore, the IBL in our case is caused by a combination of changes in surface forcing. Studies of momentum IBLs, such as the one by Glendening and Lin (2002), are caused by a change only in surface roughness. They choose to identify the top of the momentum IBL as the location of a 10% change in momentum flux from the upstream value. Studies of thermal IBLs, such as one by Venkatram (1977), usually define the top of the thermal IBL as the altitude of the potential temperature jump z_i . In those cases, the upwind boundary layer is usually

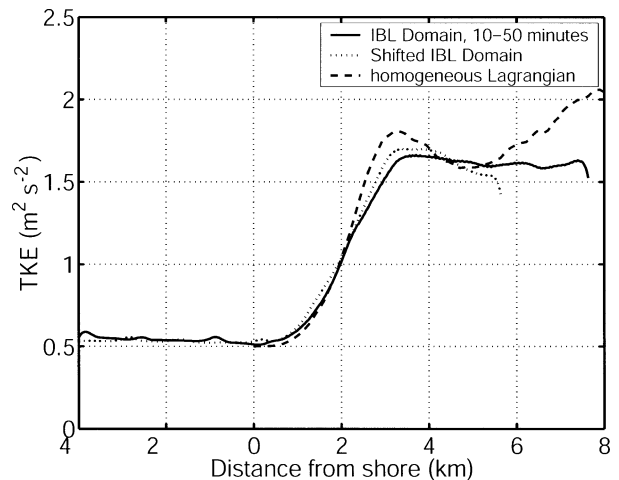


FIG. 8. Mean turbulent kinetic energy as a function of distance from the shore. The solid line is from an IBL run with a 4-km land surface and 8-km water surface. The dashed line is the mean TKE in a horizontally homogeneous LES where time was converted to offshore distance by use of a mean advection speed. The dotted line is from an IBL run with a 6-km land surface and 6-km water surface.

presumed to be stable. Since the upwind boundary layer in our case was weakly convective, the height of the capping inversion, which is straightforward to locate, is not a useful indicator of the height of the IBL. In fact, the potential temperature contours at the base of the capping inversion, in our case, slightly decrease in altitude, immediately downstream of the shoreline. Therefore, we choose not to put an exact location on the top of the IBL in the present case since the definition is somewhat arbitrary and, in the average sense, the region is characterized more by gradual changes than step changes.

It is important to note that for this experiment to be successful, the height of the domain was restricted to 1 km. Gravity waves became trapped in the inversion layer in precursor runs with deeper domains. These waves amplified over time, and in precursor simulations over several hours the waves eventually dominated the turbulent structures in the boundary layer. It is likely that gravity waves play a role in the organization of boundary layer structure (e.g., see Carruthers and Moeng 1987; Kuettner et al. 1987; Hauf and Clark 1989), and we admit that we have absorbed them by limiting the depth of our domain and installing an absorbing layer in the top. It is also important to note that the constant inflow boundary condition does not allow gravity waves to propagate upstream and therefore it places another restriction on the direction of wave propagation. Therefore, the technique may not work for some atmospheric simulations where the modeling of upstream propagating gravity waves is important.

5. Summary

The objective of this paper is to describe and demonstrate a simple method that can be used with non-

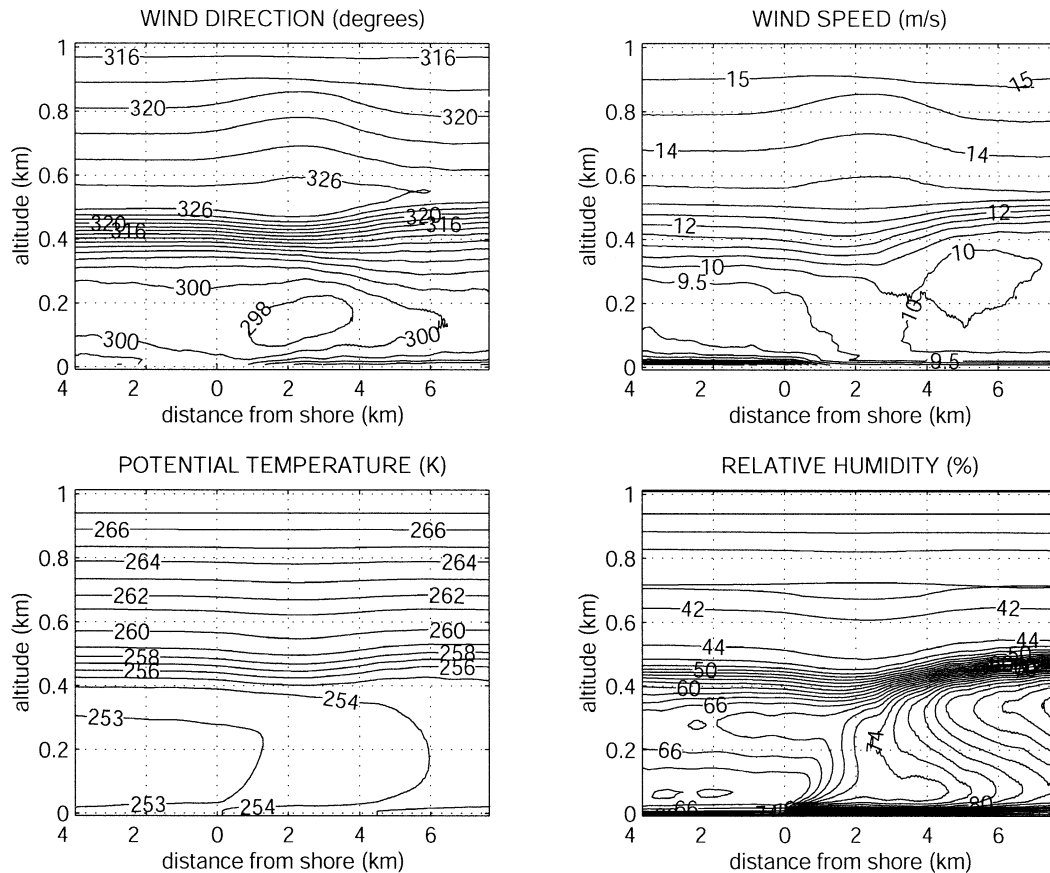


FIG. 9. Contour plots of mean wind direction (upper left), wind speed (upper right), potential temperature (lower left), and relative humidity (lower right) on vertical cross sections perpendicular to the shoreline. Model output from the last 30 min of the simulation was used to compute these mean fields.

periodic large-eddy simulation models to enable the simulation of inhomogeneous boundary layers such as mesoscale internal boundary layers. The technique worked for our particular case, but remains to be extended to situations with deeper domains, where upstream wave propagation may occur, or in environments with strong directional wind shear. Detailed features of the simulated internal boundary layer structure will be compared with lidar observations in a future paper. The authors hope that the presentation of this technique stimulates other modelers to try LESs of horizontally inhomogeneous boundary layers.

Acknowledgments. This work was started as part of the first author's dissertation research while at the University of Wisconsin. This work was funded from NSF Grants ATM9707165 and 9708314. The authors thank P. Sullivan, C.-H. Moeng, and E. Eloranta for helpful discussions about this topic and three anonymous reviewers for their very useful suggestions.

REFERENCES

Andren, A., A. R. Brown, J. Graf, P. J. Mason, C.-H. Moeng, F. T. M. Nieuwstadt, and U. Schumann, 1994: Large eddy simulation

- of a neutrally stratified boundary layer: A comparison of four computer codes. *Quart. J. Roy. Meteor. Soc.*, **120**, 1457–1484.
- Boersma, B. J., cited 1998: Direct simulation of a jet diffusion flame. Stanford University Center for Turbulence Research Annual Research Briefs. [Available online at <http://ctr.stanford.edu/ResBriefs98/boersma.pdf>.]
- Carruthers, D. J., and C.-H. Moeng, 1987: Waves in the overlying inversion of the convective boundary layer. *J. Atmos. Sci.*, **44**, 1801–1808.
- Clark, T. L., 1977: A small-scale dynamic model using a terrain-following coordinate transformation. *J. Comput. Phys.*, **24**, 186–215.
- Coleman, G. N., J. H. Ferziger, and P. R. Spalart, 1990: A numerical study of the turbulent Ekman layer. *J. Fluid Mech.*, **213**, 313–348.
- Durrant, D. R., 1981: The effects of moisture on mountain waves. NCAR Cooperative Thesis 65, 142 pp.
- , 1999: *Numerical Methods for Wave Equations in Geophysical Fluid Dynamics*. Springer-Verlag, 465 pp.
- Fedorovich, E., F. T. M. Nieuwstadt, and R. Kaiser, 2001: Numerical and laboratory study of a horizontally evolving convective boundary layer. Part I: Transition regimes and development of the mixed layer. *J. Atmos. Sci.*, **58**, 70–86.
- Garratt, J. R., 1990: The internal boundary layer—A review. *Bound.-Layer Meteor.*, **50**, 171–203.
- Glendening, J. W., 1995: Horizontally integrated atmospheric heat flux from an Arctic lead. *J. Geophys. Res.*, **100**, 4613–4620.
- , and C.-L. Lin, 2002: Large-eddy simulation of internal boundary layers created by a change in surface roughness. *J. Atmos. Sci.*, **59**, 1697–1711.

- Hack, J. J., and W. H. Schubert, 1981: Lateral boundary conditions for tropical cyclone models. *Mon. Wea. Rev.*, **109**, 1404–1420.
- Hauf, T., and T. L. Clark, 1989: Three-dimensional numerical experiments on convectively forced internal gravity waves. *Quart. J. Roy. Meteor. Soc.*, **115**, 309–333.
- Klemp, J. B., and D. K. Lilly, 1978: Numerical simulation of hydrostatic mountain waves. *J. Atmos. Sci.*, **35**, 78–107.
- , and R. B. Wilhelmson, 1978: The simulation of three-dimensional convective storm dynamics. *J. Atmos. Sci.*, **35**, 1070–1096.
- Kuettner, J. P., P. A. Hildebrand, and T. L. Clark, 1987: Convection waves: Observations of gravity wave systems over convectively active boundary layers. *Quart. J. Roy. Meteor. Soc.*, **113**, 445–467.
- Lin, C.-L., C.-H. Moeng, P. P. Sullivan, and J. C. McWilliams, 1997: The effect of surface roughness on flow structures in a neutrally stratified planetary boundary layer flow. *Phys. Fluids*, **9**, 3235–3249.
- Lund, T. S., X. Wu, and K. D. Squires, 1998: Generation of turbulent inflow data for spatially-developing boundary layer simulations. *J. Comput. Phys.*, **140**, 233–258.
- Mahrt, L., 2000: Surface heterogeneity and vertical structures of the boundary layer. *Bound.-Layer Meteor.*, **96**, 33–62.
- Mayor, S. D., and E. W. Eloranta, 2001: Two-dimensional vector wind fields from volume imaging lidar data. *J. Appl. Meteor.*, **40**, 1331–1346.
- Moeng, C.-H., 1984: A large-eddy simulation model for the study of planetary boundary layer turbulence. *J. Atmos. Sci.*, **41**, 2052–2062.
- Nieuwstadt, F. T. M., P. J. Mason, C.-H. Moeng, and U. Schumann, 1993: Large eddy simulation of the convective boundary layer: A comparison of four computer codes. *Turbul. Shear Flows*, **8**, 343–367.
- Orlanski, I., 1976: A simple boundary condition for unbounded hyperbolic flows. *J. Comput. Phys.*, **21**, 251–269.
- Pielke, R., 2001: *Mesoscale Meteorological Modeling*. Academic Press, 750 pp.
- Spalart, P. R., 1988: Direct simulation of a turbulent boundary layer up to $R_\theta = 1410$. *J. Fluid Mech.*, **187**, 61–98.
- , and J. Watmuff, 1993: Experimental and numerical study of a turbulent boundary layer with pressure gradients. *J. Fluid Mech.*, **249**, 337–371.
- Tripoli, G. J., 1992: A nonhydrostatic mesoscale model designed to simulate scale interaction. *Mon. Wea. Rev.*, **120**, 1342–1359.
- , and W. R. Cotton, 1982: The Colorado State University three-dimensional cloud/mesoscale model, Part 1: General theoretical framework and sensitivity experiments. *J. Rech. Atmos.*, **16**, 185–218.
- , and —, 1989: Numerical study of an observed orogenic mesoscale convective system. Part 1: Simulated genesis and comparison with observations. *Mon. Wea. Rev.*, **117**, 273–304.
- Venkatram, B., 1977: A model of internal boundary layer development. *Bound.-Layer Meteor.*, **11**, 419–437.